Mechanisms of slope failure on Pyramid Mountain, a subglacial volcano in Wells Gray Provincial Park, British Columbia

Daniel P. Neuffer, Richard A. Schultz, and Robert J. Watters

Abstract: Pyramid Mountain is a subglacial volcano in Wells Gray Provincial Park in east-central British Columbia. Landslides deform the north and east flanks of the volcano. Field strength testing and rock mass classification designate the hyaloclastite breccia in which the landslides originated as a weak, massive rock mass: uniaxial compressive strengths (UCS) range from 24 to 35 MPa, and geologic strength index (GSI) and rock mass rating (RMR) values are 60–70. The shear strength of fracture surfaces in the hyaloclastite breccia, as measured by laboratory direct shear tests, can be characterized by a friction angle ϕ of 18° and cohesion c of 0.11–0.66 MPa. Limit-equilibrium slope stability analyses show that the landslides were probably triggered by the rapid drawdown of a surrounding englacial lake with no seismic ground acceleration required. Slope measurements and slope stability modeling indicate that Pyramid Mountain was asymmetric prior to failure: the north and east flanks had slope angles of 35°–40°, and the south and west flanks had slope angles of 21°–33°. Slope asymmetry may result from closer ice confinement on up-gradient (north and east) flanks due to higher ice flux in this direction relative to down-gradient (south and west) flanks. At the time of failure, the volcanic edifice was at least partially lithified, with cohesive strengths of 0.19–0.52 MPa. Failures of lithified subglacial and subaqueous volcanic edifices may be triggered by rapid drawdown of surrounding water without seismic loading.

Résumé : Le mont Pyramid est un volcan infraglaciaire du parc provincial Wells Gray, dans le centre-est de la Colombie-Britannique. Les flancs nord et est du volcan sont déformés par des glissements de terrain. Selon des essais de résistance effectués sur le terrain et la classification de la masse rocheuse, la brèche de hyaloclastite, où les glissements de terrain ont pris naissance, est un amas rocheux massif et faible : la résistance à la compression uniaxiale varie entre 24 MPa et 35 MPa, tandis que les valeurs fournies par l'indice GSI (« Geologic Strength Index ») et le système RMR (« Rock Mass Rating ») se situent entre 60 et 70. La résistance au cisaillement des surfaces de fracture de la brèche de hyaloclastite, telle que mesurée en laboratoire par des essais de cisaillement direct, se caractérise par un angle de frottement (ϕ) = 18° et une cohésion (c) = 0,11–0,66 MPa. Des analyses de stabilité des pentes selon une méthode de calcul à l'équilibre limite indiquent que les glissements de terrain ont probablement été provoqués par le rabattement rapide d'un lac intraglaciaire environnant, sans intervention de mouvement sismique. Les mesures des pentes et la modélisation de la stabilité des pentes indiquent qu'avant l'effondrement, le mont Pyramid était asymétrique : les pentes des flancs nord et est étaient comprises entre 35° et 40° et celles des flancs sud et ouest étaient comprises entre 21° et 33°. Cette asymétrie des pentes pourrait être le résultat d'une plus grande proximité du confinement de la glace sur les flancs amont (nord et est), imputable au plus grand écoulement glaciaire dans cette direction, que sur les flancs aval (sud et ouest). Au moment de l'effondrement, l'édifice volcanique était au moins partiellement lithifié et possédait une force de cohésion variant entre 0,19 MPa et 0,52 MPa. Les effondrements des édifices volcaniques infraglaciaires et subaquatiques lithifiés pourraient avoir été provoqués par le rabattement rapide de l'eau environnante, sans charge sismique.

[Traduit par la Rédaction]

Introduction

Basaltic volcanoes have erupted beneath glaciers or ice sheets in British Columbia (e.g., Mathews 1947; Allen et al. 1982; Hickson and Souther 1984; Hickson 1987, 2000; Hickson et al. 1995), Iceland (e.g., Van Bemmelen and Rutten 1955; Jones 1969, 1970; Gudmundsson et al. 1997, 2002, 2004; Werner and Schmincke 1999), Antarctica (e.g., Smellie et al. 1993; Smellie and Skilling 1994; Skilling 1994; Smellie and Hole 1997; Smellie 2000, 2002; Le Masurier 2002), and Siberia

Received 31 March 2005. Accepted 24 October 2005. Published on the NRC Research Press Web site at http://cjes.nrc.ca on 13 March 2006.

Paper handled by Associate Editor R. Gilbert.

D.P. Neuffer[1,2], R.A. Schultz, and R.J. Watters. Geological Engineering Program, Department of Geological Sciences and Engineering, Mackay School of Earth Sciences and Engineering, University of Nevada, Reno, NV 89557-0138, USA.

[1]Present address: RTW Professional Engineers and Consultants, Inc., 825 Railroad St., Elko, NV 89801, USA.
[2]Corresponding author (e-mail: DPN@rtweng.com).

 doi:10.1139/E05-100

(e.g., Komatsu et al. 2004). Slope failures on subglacial volcanoes have been noted by many of the aforementioned workers; based on stratigraphic and structural observations. Smellie and Skilling (1994), Skilling (1994), Smellie and Hole (1997), Smellie (2000), and Le Masurier (2002) describe slope failures on subglacial volcanoes ranging from small-scale soft-sediment slumps to partial collapse of the lithified volcanic edifice. Excess pore pressure generation and over-steepening during volcanic construction (Smellie and Skilling 1994; Smellie and Hole 1997; Smellie 2000), seismic loading (Smellie and Skilling 1994; Smellie and Hole 1997), rapid drawdown of the surrounding englacial lake (Hickson 1987; Skilling 1994), hydrothermal alteration (Skilling 1994), and removal of buttressing ice (Hickson et al. 1995, 2000; Smellie and Hole 1997) are cited as possible mechanisms of large-scale slope failure on subglacial volcanoes. Landslides on subglacial volcanoes have not been mechanically analyzed, however, to determine the most probable causes of failure.

This work utilizes landslide mapping, field and laboratory measurements of rock mass strength, and limit-equilibrium slope stability analysis to examine the roles of lithification, slope geometry, hydrologic conditions, and seismic loading in initiating edifice failure on Pyramid Mountain, a subglacial volcano in Wells Gray Provincial Park, British Columbia. Slope stability modeling shows that landslides on the north and east flanks of Pyramid Mountain most likely occurred during rapid drawdown of an englacial lake surrounding a partially to fully lithified edifice with no seismic loading necessary. In addition, Pyramid Mountain was asymmetric prior to failure, with slope angles of 35°–40° on the north and east flanks and 21°–33° on the south and west slopes of the mountain.

Study area

Pyramid Mountain is a subglacial volcano in the Wells Gray – Clearwater volcanic field, a Pliocene to Holocene volcanic complex in east-central British Columbia (Fig. 1) (Hickson et al. 1995). The volcanic field is located in the Quesnel – Shuswap Highlands physiographic region, a dissected plateau that lies between the Interior Plateau to the west and the Columbia Mountains to the east (Fig. 1) (Hickson et al. 1995). Underlain primarily by Precambrian metamorphic rocks, the Wells Gray – Clearwater volcanic field comprises alkali olivine basalts erupted in subaerial, subaqueous, and subglacial environments (Hickson and Souther 1984). The Wells Gray – Clearwater area is situated at the transition between north- and northwest-trending structures (Hickson 1987). Pyramid Mountain and much of the volcanic field are located in the post-Miocene Clearwater Depression (Hickson 1987), a possible graben formed in the overlap region of two inferred north-trending normal faults (Fig. 1).

From at least 20 to 11 ka, the Fraser Glaciation covered the Wells Gray – Clearwater region with a continental ice sheet that reached maximum elevations of 2400 m, inundating many of the ridges and peaks in the area (Hickson et al. 1995). Pyramid Mountain was formed by subglacial eruption, probably during the late stages of the Fraser Glaciation (Hickson 1987). At the time of eruption, glacial ice was at least 500 m thick in the area (Hickson et al. 1995) and moved from northeast to southwest, creating morainal ridges, kame fields, and eskers on a gently sloping Pleistocene lava surface (Hickson and Souther 1984). This lava surface has been deeply incised by the Clearwater River to the west but remains largely undissected by the Murtle River, which flows from the north-east past Pyramid Mountain to join the Clearwater River (Figs. 1, 2A) (Hickson and Souther 1984).

Methods

Landslides on Pyramid Mountain were mapped on a 1 : 12 000 scale topographic map (Fig. 3) generated from a 1 : 50 000 scale digital elevation model (DEM) of the area (Geobase 2004). Mapping was based on reconnaissance field-work, low-altitude aerial overflights, and photographs taken during the aerial overflights. Due to limited exposures, bedding attitudes and geomechanical data were collected at several outcrops of hyaloclastite breccia on the east and west flanks of the mountain (Figs. 2B, 3). Geomechanical characterization followed procedures outlined by the International Society for Rock Mechanics Commission on Standardization of Laboratory and Field Tests (1978). A Schmidt hammer was used to measure uniaxial compressive strength (UCS) according to Ege et al. (1970). Geologic strength index (GSI) was determined graphically (Hoek and Brown 1997) and quantitatively (Sonmez and Ulusay 1999). Rock mass rating (RMR) was calculated following the methods of Bieniawski (1976, 1989). GSI and RMR are estimates of rock mass strength and, along with UCS and m_i (a material constant), are inputs for the Hoek–Brown strength criterion, from which rock mass shear strength can be determined (Hoek et al. 2002).

Laboratory direct shear testing was performed on two samples of hyaloclastite breccia from Pyramid Mountain to assess the Mohr–Coulomb shear strength of fractures in the rock material. The friction angle (ϕ) for a fracture surface represents a lower-bound estimate of ϕ for the intact rock (Lockner 1995) and rock mass. Sample PM-001 was tested as an intact sample and then sheared along the resulting failure plane at five levels of normal stress. Sample PM-002 was sheared along an artificial fracture surface at five levels of normal stress (Fig. 4A).

Pyramid Mountain

Geomorphology

Pyramid Mountain is a roughly conical volcano with a summit elevation of ~1100 m, giving a maximum relief of ~260 m above the Murtle River (Fig. 3). The volume of Pyramid Mountain is ~0.1 km^3. Average slope angles range from ~21° to 27° for the south and west flanks (intact slopes) of the mountain and from ~27° to 35° (up to 67% steeper than the south and west aspects) for the north and east flanks (including failed and intact slopes). Preliminary slope measurements on McLeod Hill and Gage Hill (Fig. 1), two subglacial volcanoes northeast of Pyramid Mountain, indicate that the northeast and east slopes of these mountains are 67% and 75% steeper than the southwest and west slopes, respectively.

A landslide scarp cuts the east flank of Pyramid Mountain and is apparently truncated by a larger, composite landslide scarp that scallops the north flank of the mountain (Figs. 2A, 3). Three major landslide deposits are evident at the bases of the

Fig. 1. Generalized geology and location of the Wells Gray – Clearwater volcanic field. Modified from Hickson et al. (1995) and Hickson (1987).

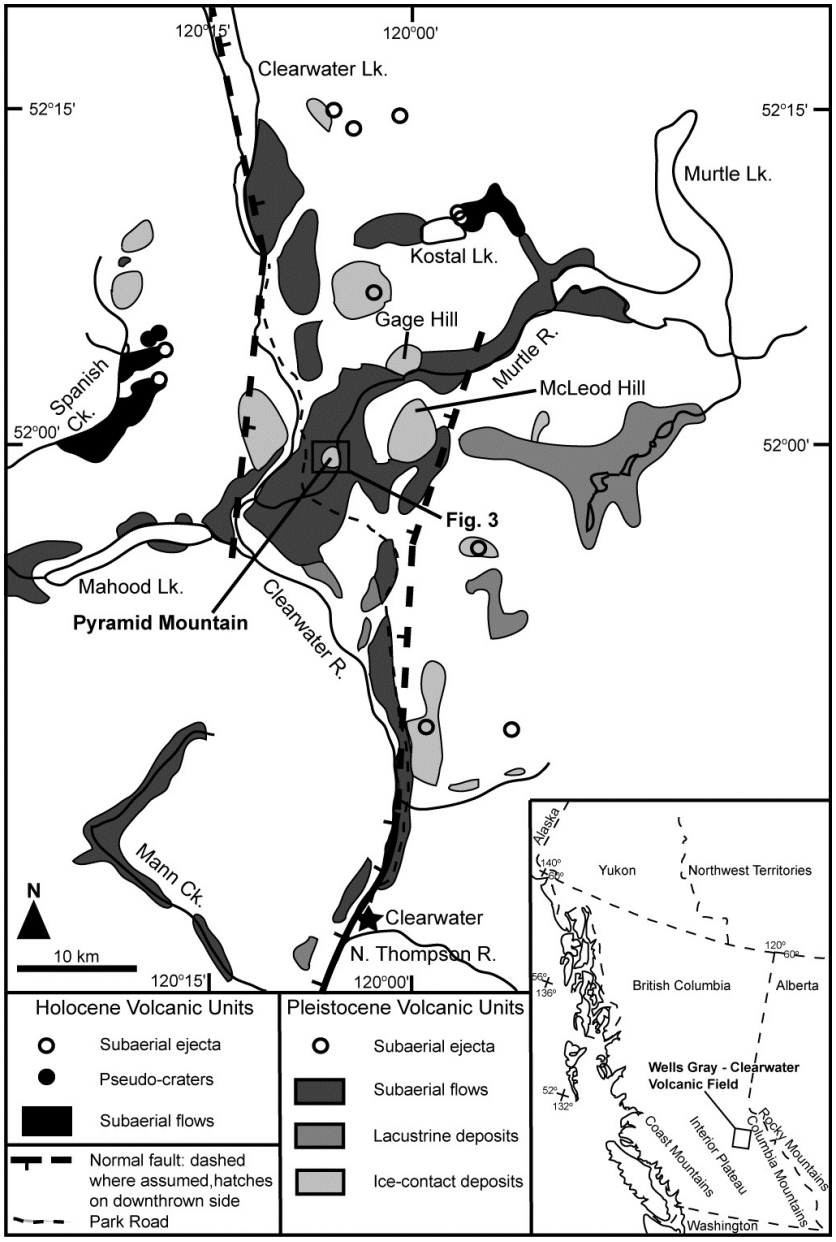

scarps (Figs. 2A, 3). The landslide deposit on the east slope of Pyramid Mountain forms a prominent bench that was interpreted by Campbell and Tipper (1971) to be a possible secondary eruptive vent but was later described by Hickson and Souther (1984), Hickson (1987), and Hickson et al. (1995) as a slump caused by the removal of surrounding water or ice. The landslide deposit on the north side of the mountain appears to have been partially removed by erosion. Although each deposit may represent multiple episodes of slope failure, the deposit on the east flank appears to be the oldest, with the deposits becoming successively younger counterclockwise around the mountain. Morainal ridges and meltwater channels from the Fraser Glaciation surround and overlap the base of Pyramid Mountain (Hickson and Souther 1984; Hickson 1987). Eskers containing laminated coarse sands and diamictons with subangular to subrounded clasts up to 7 cm in diameter occur to the north of Pyramid Mountain (Hickson 1987; Hickson et al. 1995).

Lithology and structure

Surface outcrops on Pyramid Mountain expose crudely bedded hyaloclastite breccia (Fig. 2B) composed of frothy, glassy basalt clasts and angular pillow lava fragments in a sparse sideromelane matrix (Hickson and Souther 1984; Hickson et al. 1995). The gas content of the basalt clasts indicates that the ejecta were erupted in shallow water within an ice sheet at least 500 m thick (Hickson et al. 1995). Clasts are mostly gravel sized but range in diameter from 0.1 to 30 cm. Palagonite alteration of the hyaloclastite is widespread but varies in degree from slight to moderate. Sample

Fig. 2. Pyramid Mountain. (A) Aerial view from the southeast. Solid lines and outlined areas denote landslide scarp and deposit locations, respectively. Arrows show approximate direction of landslide movement. (B) Steeply dipping beds of hyaloclastite breccia on the failed east flank of Pyramid Mountain. View is to the southwest, with a 1 m hiking pole for scale.

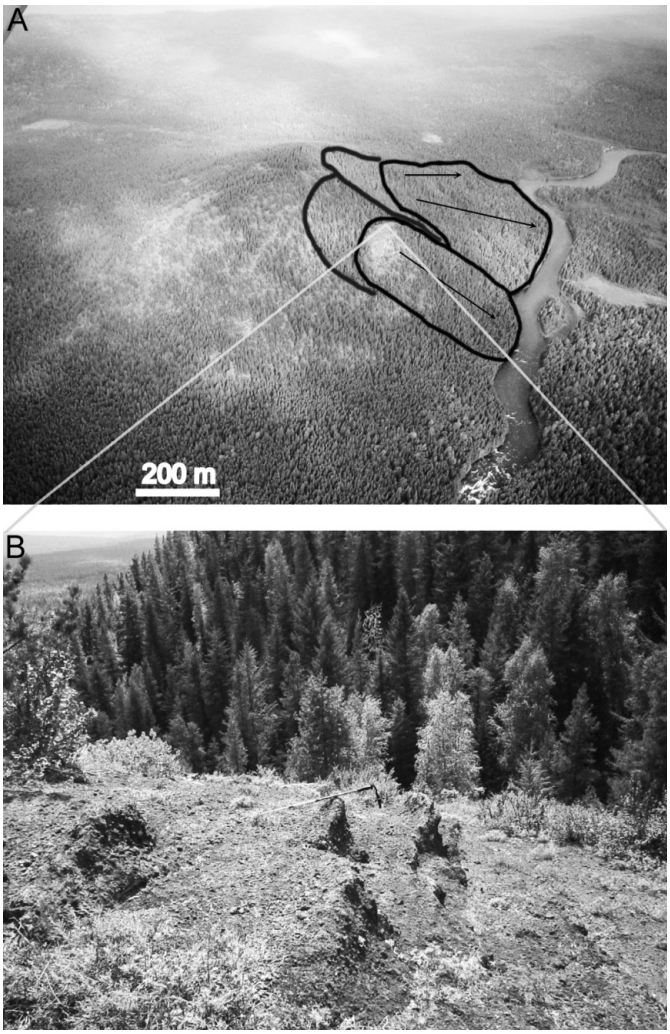

Fig. 3. Landslide map of Pyramid Mountain. Solid lines and patterned areas denote main scarps and landslide deposits, respectively. Contour interval = 10 m. Structural measurements indicate outcrop locations. Sample PM-001 was taken near bedding attitude measurement on west flank, and sample PM-002 near fracture attitude measurement on east flank. Slope profiles A–A′, B–B′, and C–C′ discussed in the text.

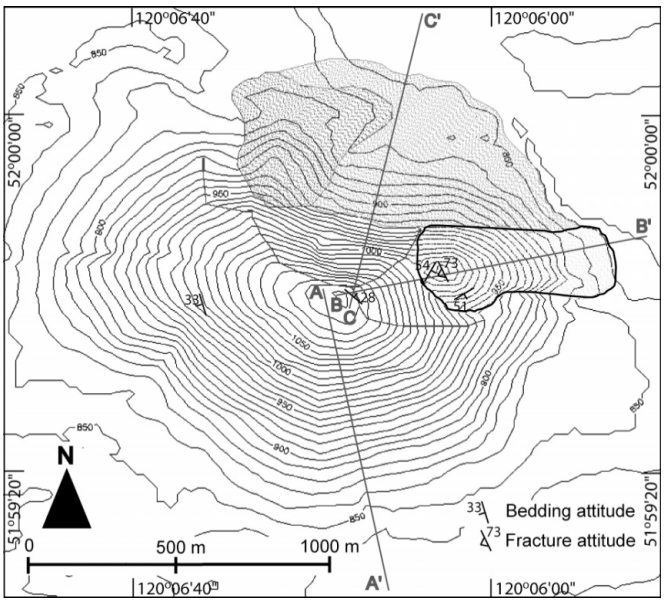

PM-001, taken on the west flank of the mountain (Fig. 3), is slightly altered hyaloclastite consisting primarily of sand-sized basalt clasts. Sample PM-002, taken on the east flank of the mountain (Fig. 3), is moderately altered hyaloclastite consisting primarily of gravel-sized basalt clasts (Fig. 4B). Shallow test pits dug by Hickson and Souther (1984) revealed slope-parallel bedding with dips averaging 26°, except on the east flank of the mountain, where significantly steeper dips were encountered. Structural measurements at nine locations confirm that bedding dips are parallel to the slopes of Pyramid Mountain (Fig. 3), except on the east bench, where dips range from 51° to 58° SE (with one measurement of 69° SE), and are consistently oblique to the overall slope (Fig. 3). The thickness of the hyaloclastite breccia and whether or not pillow lava exists at depth are unknown. Surface outcrops of hyaloclastite breccia on Pyramid Mountain are virtually unfractured. At the top of the east bench, a poorly exposed fracture with a surface trace of ~20 m dips steeply into the slope (Fig. 3).

Geomechanical properties

Rock mass classification of the hyaloclastite breccia on Pyramid Mountain yielded a graphical GSI of 65–70, a quantitative GSI of 60–66, and an RMR of 67–69. The dry bulk density of sample PM-001 is 1.6 g·cm^{-3}. UCS for the hyaloclastite breccia is 24 MPa for moderately altered rock and 35 MPa for slightly altered rock. Given the low intact UCS and lack of discontinuities, the hyaloclastite breccia can be characterized as a "massive, weak rock mass" (Hoek 2000). Using the lower-bound strength estimates of GSI = 60 and UCS = 24 MPa and an m_i value of 18 (Hoek and Brown 1997), minimum Hoek–Brown and equivalent Mohr–Coulomb rock mass strength parameters were calculated for the hyaloclastite breccia. Tensile strength, UCS, and deformation modulus for the rock mass are –0.065 MPa, 2.57 MPa, and 8.71 GPa, respectively. Assuming an upper-bound minimum principal stress corresponding to a 260 m high slope (Hoek et al. 2002), the average friction angle (ϕ) and cohesion (c) of the hyaloclastite breccia rock mass are 44° and 1.08 MPa, respectively. This shear strength is consistent with intact hyaloclastite shear strengths reported by Ishijima and Fujii (1997). Direct shear tests indicate that the shear strength of fracture surfaces in the hyaloclastite breccia can be characterized by a friction angle ϕ of 18° and cohesion c of 0.11–0.66 MPa (Fig. 4B), although more testing is required for definitive values. The high surface roughness resulting from the coarser particle size of PM-002 is almost certainly responsible for the larger apparent cohesion value relative to the finer grained PM-001.

Fig. 4. Laboratory direct shear tests. (A) Sample of PM-002 in direct shear apparatus after shear testing. Penny for scale. (B) Mohr–Coulomb strength envelopes for fracture surfaces in PM-001 and PM-002.

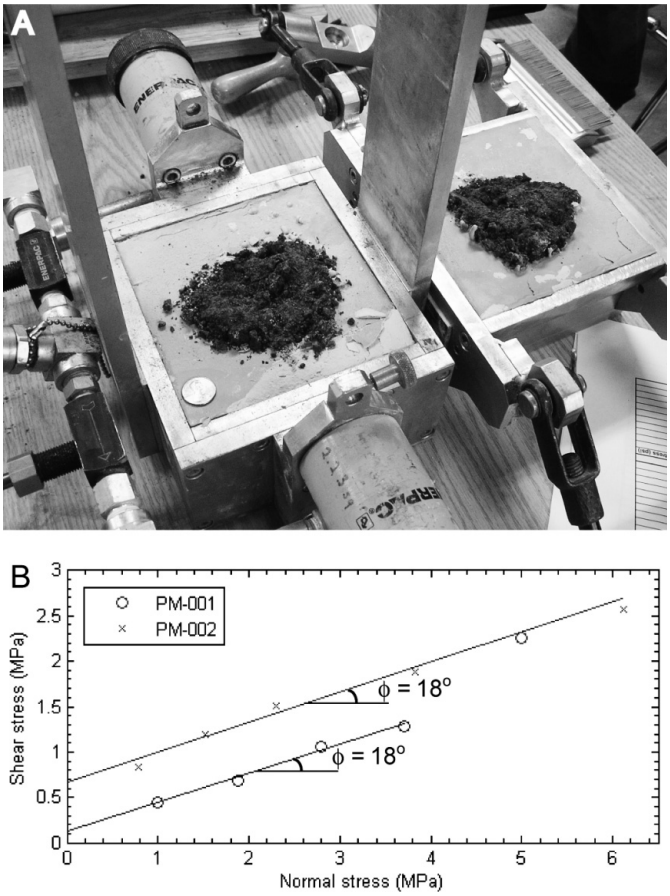

Slope stability modeling

Methods

Limit-equilibrium analysis is commonly used in geotechnical engineering to assess the stability of slopes. If the geometry, material strengths, pore-pressure conditions, and seismic loading (where applicable) are known for a given slope, the safety factor (SF) for that slope can be determined. The SF is the ratio of forces resisting movement to the forces driving movement of the portion of a slope that is most prone to fail. Hence, slopes with an SF < 1 are unstable, and slopes with an SF > 1 are stable. Limit-equilibrium back-analysis is used to determine the conditions at the time of failure by computing the slope geometry, material strengths, hydrologic conditions, or ground acceleration necessary for an SF = 1.

Circular failure occurs in slopes comprising soil, weak rock, or heavily fractured rock (Hoek and Bray 1981). As described previously, hyaloclastite breccia on Pyramid Mountain is weak, massive rock; furthermore, landslide scarps on the mountain are spoon-shaped, a common trait of rotational slides (Cruden and Varnes 1996). Therefore, circular failure was the most probable mode of landslide initiation on Pyramid Mountain. Slide 5.0 is a slope stability program produced by Rocscience Inc. that uses two-dimensional limit-equilibrium analysis to determine the SF for landslides with circular failure surfaces. Utilizing Slide 5.0, we back-analyzed slopes on Pyramid Mountain to determine if the hyaloclastite was lithified or unlithified at the time of slope failure and the respective roles of water and seismic loading in landslide initiation.

Back-analyses were performed for several slope geometry scenarios: (1) intact southeast slope of Pyramid Mountain (profile A–A′ in Fig. 3); (2) failed east slope of Pyramid Mountain (profile B–B′ in Fig. 3); (3) failed north slope of Pyramid Mountain (profile C–C′ in Fig. 3); and (4) estimated prefailure slopes for the east and north slopes of Pyramid Mountain (260 m high slopes analyzed at slope angles ranging from 30° to 45°).

Back-analyses were performed using three material strength scenarios (unit weight was held constant at 1600 $kN \cdot m^{-3}$ for all scenarios): (1) for a given set of external conditions, unlithified hyaloclastite was simulated by setting $c = 0$ and determining ϕ for an SF of 1.00; (2) the shear strength of the current lithified rock mass was represented by the Hoek–Brown strength parameters described previously (UCS = 24 MPa, GSI = 60, $m_i = 18$); (3) the shear strengths of fracture surfaces in hyaloclastite breccia obtained through direct shear testing ($\phi = 18°$, $c = 0.11$–0.66 MPa).

Back-analyses were performed using several hydrologic scenarios: (1) dry slope; (2) submerged slope, in which the entire slope is underwater; (3) complete, rapid drawdown of the englacial lake simulated by two methods, namely (*i*) all external water has been removed, but the slope remains saturated (Walker and Santi 2004) and (*ii*) "rapid drawdown" setting in Slide 5.0 with Skempton's coefficient for slope material set to one; (4) partial, rapid drawdown (simulated water table at successive stages of rapid drawdown intermediate between scenarios 2 and 3).

With the exception of the "dry" case, groundwater scenarios representative of subaerial conditions were not modeled because the superposition of glacial deposits on landslide deposits at the base of Pyramid Mountain precludes postglacial failure. Dry conditions are unlikely because an englacial landslide requires a cavity to accommodate mass movement; a cavity that is not at least initially water-filled will rapidly close due to ice inflow (Höskuldsson and Sparks 1997). For a given combination of slope geometry, material strength, and water conditions, the effect of seismic loading on slope stability was determined by varying the horizontal ground acceleration from 0 to 1*g* on the most critical failure surface. Slide 5.0 approximates ground acceleration as a horizontal force acting on the potential failure mass (pseudo-static analysis).

Results

Over 70 Slide 5.0 models were computed for the slope geometries, material strengths, hydrologic conditions, and seismic loads described previously. The following modeling scenarios produce failure of the north and east flanks and stability of the south and west flanks, and hence align with observations of Pyramid Mountain:

(1) All current slopes are stable for lithified hyaloclastite (i.e., current Hoek–Brown rock mass shear strengths)

Fig. 5. Slide 5.0 models of Pyramid Mountain. No vertical exaggeration. (A) Most critical failure surface and SF for the current (lithified, failed) east slope after rapid and complete drawdown of surrounding water (fully saturated conditions). (B) One hundred most critical failure surfaces and most critical SF for a lithified, 40° slope after rapid and complete drawdown of surrounding water. (C) Most critical failure surface and SF for a lithified, 30° slope after rapid and complete drawdown of surrounding water. (D) Most critical failure surface and SF for the same slope depicted in (B) but fully submerged. A horizontal ground acceleration of at least 0.47 *g* is required for failure. (E) Most critical failure surface and SF for the unlithified ($\phi = 58^{\circ}$, $c = 0$), intact southeast slope after rapid and complete drawdown of surrounding water. (F) Most critical failure surface and SF for the current (lithified, intact) southeast slope after rapid and complete drawdown of surrounding water. A horizontal ground acceleration of 0.40 *g* is required for failure.

undergoing rapid drawdown of a surrounding lake (Fig. 5A).

(2) Saturated, lithified, 260 m high slopes with angles of 35°–40° will fail during rapid drawdown of a surrounding lake with no horizontal ground acceleration (Fig. 5B).

(3) For the laboratory shear strength of $\phi = 18°$ and $c = 0.66$ MPa, slope angles > 45° are required for failure of a saturated, 260 m high slope with no ground acceleration.

(4) For a 260 m high, 35°–40° slope and rapid drawdown conditions, the cohesive strength of the edifice at failure was 0.19–0.52 MPa for a range of $\phi = 18–50°$. The lower-bound ϕ value is from the laboratory direct shear tests; the upper-bound ϕ value is a maximum for intact basalt (Rahn 1996).

The following modeling scenarios do not cause landslide initiation on estimated prefailure slopes for the north and east flanks of Pyramid Mountain and thus do not match observations:

(1) Lithified slopes that are 260 m high with slope angles < 35° are stable during rapid drawdown (Fig. 5C).

(2) Submerged, lithified, 260 m high slopes with angles of 30°–40° will not fail at horizontal ground accelerations of < 0.47*g* (Fig. 5D). The peak horizontal ground acceleration (with 10% probability of exceedance in 50 years) in the area is 0.04*g*–0.08*g* (Geological Survey of Canada 2004), significantly lower than the seismic load required for failure in submerged, lithified conditions.

The following modeling scenarios result in failure of the intact south and west flanks of Pyramid Mountain and therefore do not correspond to observations:

(1) For $\phi < 58°$, cohesionless, unlithified, saturated materials cause failure of intact slopes (Fig. 5E). For natural cohesionless soils, typical ϕ values range from 28° to 46°, depending on density (Holtz and Kovacs 1981).

(2) The laboratory shear strength of $\phi = 18°$ and $c = 0.11$ MPa causes failure of saturated, intact slopes. This shear strength also results in an SF of 1.07 for the current topography of the east flank under dry conditions, implying that this shear strength is probably too low to be representative of the hyaloclastite rock mass.

(3) Current intact slopes will fail in a lithified condition only during rapid drawdown with a simultaneous horizontal ground acceleration of > 0.40*g*, an unlikely condition (Fig. 5F).

Discussion and implications

Simple circular failures cause surfaces in the main body of a landslide to rotate toward the main scarp, often leading to beds in the landslide deposit that dip less steeply than or in the opposite direction from beds in the intact slope. Toppling failures can result in bedding that dips more steeply in the toppled block than in the intact slope. Bedding attitudes at the top of the east landslide deposit are steeper than those on the intact slope directly above the landslide (Fig. 3), implying that toppling was the failure mode for the east slope. The arcuate geometry of the main scarp of the east flank landslide indicates circular failure, however. Two possible scenarios account for both the bedding attitudes and circular failure of the east slope:

(1) The east slope may have failed initially as a circular failure, followed by a slide head topple. A slide head topple occurs when a portion of the steep main scarp slope, exposed by a circular, planar, or wedge failure, topples onto the head of the landslide deposit (Hoek and Bray 1981).

(2) Alternatively, the eruption products may have been originally deposited at angles of 50°–60° due to deposition against ice or infilling of a prelithification landslide scar. Following eruption and some lithification, the east flank was deformed by a circular failure that produced minimal back-rotation during sliding. The slope stability modeling approach is valid for either failure scenario.

The most probable failure scenario for the north and east flanks of Pyramid Mountain is shown in Fig. 6 and described as follows:

(1) A basaltic subglacial volcanic eruption produces Pyramid Mountain below a minimum ice thickness of 500 m. Meltwater probably drains away continuously during the eruption (i.e., Gudmundsson et al. 2004). The volcano is asymmetric in slope, with the steeper (north and east) flanks facing up-gradient relative to the direction of ice flow and the shallower (south and west) flanks facing down-gradient. Slope asymmetry may result from closer ice confinement on up-gradient flanks due to higher ice flux in this direction relative to down-gradient flanks. Glacial erosion of a rock protrusion results in a gentle up-gradient slope and a steep down-gradient slope (e.g., Dolgoff 1996; Ritter et al. 1995), the opposite of what is observed on Pyramid Mountain and other nearby subglacial volcanoes.

(2) The volcanic eruption ceases, but the volcanic pile retains heat for years, which together with abundant meltwater causes palagonitization and partial lithification of the edifice in as little as 1–2 years (i.e., Fisher and Schmincke 1984; Gudmundsson et al. 2002). The edifice becomes flooded with water and possibly overrun with ice (i.e., Gudmundsson et al. 2002).

(3) Opening or enlargement of subglacial drainage tunnels causes rapid drawdown of the englacial lake, resulting in failure of the 35°–40°, saturated, unsupported north and east slopes of Pyramid Mountain. The south and

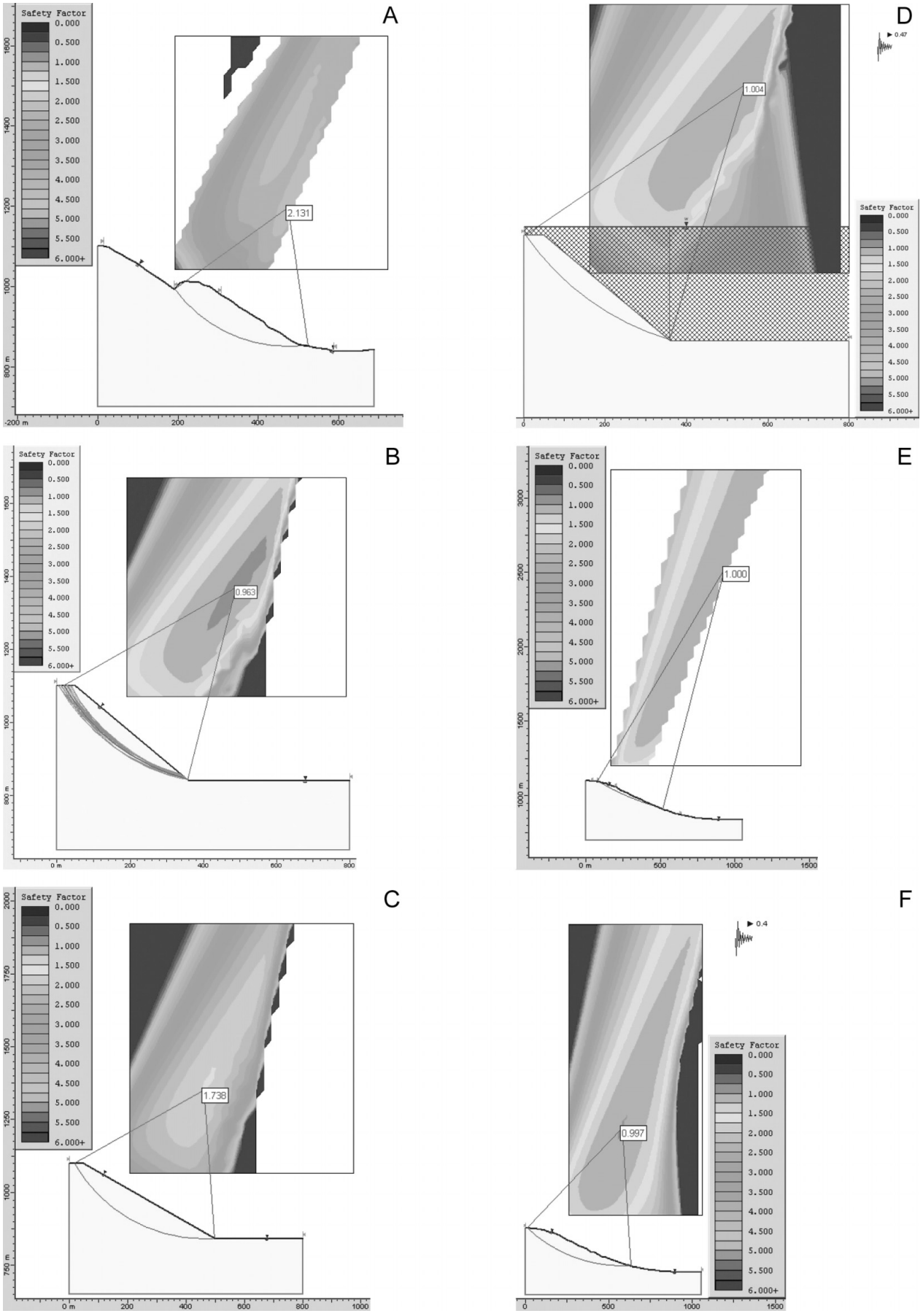

Fig. 6. Estimated conditions on Pyramid Mountain and surroundings (A) immediately prior to slope failure and (B) immediately after slope failure.

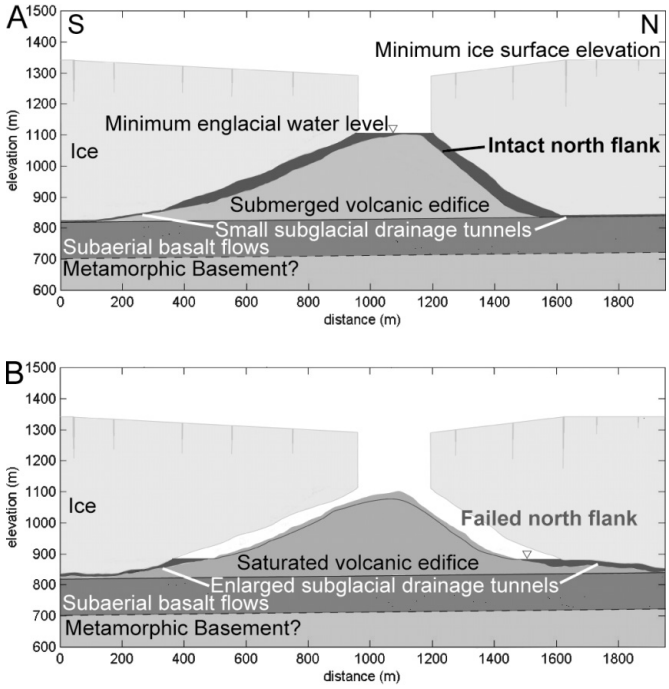

west slopes remain intact due to lower slope angles of 21°–33°.

The failure of the north and east flanks of Pyramid Mountain following at least partial lithification is supported by the observations that the landslide deposit on the east flank is a coherent block with no evidence of soft-sediment deformation and by the absence of eruption products overlying the landslides. Furthermore, slope stability modeling showed that the geometry of failure surfaces in lithified materials more closely matches the observed scarp geometries, whereas failure surfaces in cohesionless materials tend to be very shallow. Failure of the north and east slopes during rapid drawdown of a surrounding englacial lake is supported by the meltwater channels that surround the base of the volcano and the eskers to the north of Pyramid Mountain (Hickson 1987). Structural and (or) alteration features (e.g., fractures, contacts with underlying units, varying degrees of alteration) that differ from observed surface outcrops may have played a role in the slope failures on Pyramid Mountain, but subsurface exploration would be necessary to determine the importance of these factors.

Conclusions

The north and east flanks of Pyramid Mountain, a subglacial volcano in east-central British Columbia, have been deformed by landslides. The hyaloclastite breccia in which the landslides originated is a weak, massive rock mass with UCS values of 24–35 MPa and GSI–RMR ratings of 60–70. The shear strength of fracture surfaces in the hyaloclastite breccia can be characterized by a friction angle ϕ of 18° and cohesion c of 0.11–0.66 MPa.

Limit-equilibrium slope stability analyses show that the north and east flanks of Pyramid Mountain probably failed during the rapid drawdown of a surrounding englacial lake, with no ground acceleration required. Slope measurements and slope stability modeling indicate that, prior to failure, Pyramid Mountain was asymmetric: the north and east flanks had slope angles of 35°–40°, and the south and west flanks had slope angles of 21°–33°. Slope asymmetry may result from closer ice confinement on up-gradient (north and east) flanks due to higher ice flux in this direction relative to down-gradient (south and west) flanks. At the time of failure, the volcanic edifice was at least partially lithified, with cohesive strengths of 0.19–0.52 MPa. Failures of lithified subglacial and subaqueous volcanic edifices may be triggered by rapid drawdown of surrounding water without seismic loading.

Acknowledgments

Support for this study was provided by the Planetary Geology and Geophysics Program of the National Aeronautics and Space Administration. The authors thank R. Routledge and B.C. Parks for their assistance in obtaining a research permit for Wells Gray Provincial Park. C. Hickson provided clarification and insight about the geology of Pyramid Mountain and a helpful review. Thanks also to R. Gilbert and an anonymous referee for their time reviewing the manuscript. J. Daemen gave useful insights on laboratory testing. DPN thanks C. Neuffer for field assistance, K. Katzenstein for contributing time and knowledge to laboratory testing, and the Schaer family at Wells Gray Air Services for the charter flight.

References

Allen, C.C., Jercinovic, M.J., and Allen, J.S.B. 1982. Subglacial volcanism in north-central British Columbia and Iceland. Journal of Geology, **90**: 699–715.

Bieniawski, Z.T. 1976. Rock mass classification in rock engineering. *In* Exploration for rock engineering: Proceedings of the Symposium on Exploration for Rock Engineering, Johannesburg, South Africa, 1–5 November 1976. A.A. Balkema, Rotterdam, The Netherlands, Vol. 1, pp. 97–106.

Bieniawski, Z.T. 1989. Engineering rock mass classifications. John Wiley and Sons, Inc., New York.

Campbell, R.B., and Tipper, H.W. 1971. Geology of Bonaparte Lake Map-Area, British Columbia. Geological Survey of Canada, Memoir 363.

Cruden, D.M., and Varnes, D.J. 1996. Landslide types and processes. *In* Landslides: investigation and mitigation. *Edited by* A.K. Turner and R.L. Schuster. National Research Council, Transportation Research Board, Washington, D.C., Special Report 247, pp. 36–75.

Dolgoff, A. 1996. Physical geology. D.C. Heath and Company, Lexington, Mass.

Ege, J.R., Miller, D.R., and Danilchik, W. 1970. Schmidt hammer tests for field determination of physical properties of zeolitized tuff. US Geological Survey, Open-file Report 70-117.

Fisher, R.V., and Schmincke, H.-U. 1984. Pyroclastic rocks. Springer-Verlag, New York, N.Y.

Geobase. 2004. Canadian digital elevation data [online]. Centre for Topographic Information, Natural Resources Canada, Ottawa, Ont. Available from http://www.geobase.ca [accessed June–July 2004].

Geological Survey of Canada. 2004. Acceleration seismic zoning map [online]. Geological Survey of Canada, Ottawa, Ont. Available from http://www.pgc.nrcan.gc.ca/seismo/eqhaz/seishaz.htm [cited August 2004].

Gudmundsson, M.T., Sigmundsson, F., and Björnsson, H. 1997. Ice–volcano interaction of the 1996 Gjálp subglacial eruption, Vatnajökull, Iceland. Nature (London), **389**: 954–957.

Gudmundsson, M.T., Pálsson, F., Björnsson, H., and Högnadóttir, T. 2002. The hyaloclastite ridge formed in the subglacial 1996 eruption in Gjálp, Vatnajökull, Iceland: present day shape and future preservation. *In* Volcano–ice interactions on Earth and Mars. *Edited by* J.L. Smellie and M.G. Chapman. Geological Society (of London) Special Publication 202, pp. 319–335.

Gudmundsson, M.T., Sigmundsson, F., Björnsson, H., and Högnadóttir, T. 2004. The 1996 eruption at Gjálp, Vatnajökull ice cap: efficiency of heat transfer, ice deformation, and subglacial water pressure. Bulletin of Volcanology, **66**: 46–65.

Hickson, C.J. 1987. Quaternary volcanism in the Wells Gray – Clearwater area, east central British Columbia. Ph.D. thesis, The University of British Columbia, Vancouver, BC.

Hickson, C.J. 2000. Physical controls and resulting morphological forms of Quaternary ice-contact volcanoes in western Canada. Geomorphology, **32**: 239–261.

Hickson, C.J., and Souther, J.G. 1984. Late Cenozoic rocks of the Clearwater – Wells Gray area, British Columbia. Canadian Journal of Earth Sciences, **21**: 267–277.

Hickson, C.J., Moore, J.G., Calk, L., and Metcalfe, P. 1995. Intraglacial volcanism in the Wells Gray – Clearwater volcanic field, east-central British Columbia. Canada. Canadian Journal of Earth Sciences, **32**: 838–851.

Hoek, E. 2000. Practical rock engineering [online]. Rocscience Inc., Toronto, Ont. Available from http://www.rocscience.com/hoek/PracticalRockEngineering.asp [cited October 2004].

Hoek, E., and Bray, J. 1981. Rock slope engineering. Institution of Mining and Metallurgy, London.

Hoek, E., and Brown, E.T. 1997. Practical estimates of rock mass strength. Journal of Rock Mechanics and Mining Sciences, **34**: 1165–1186.

Hoek, E., Carranza-Torres, C., and Corkum, B. 2002. Hoek–Brown failure criterion — 2002 edition. *In* Mining and tunnelling innovation and opportunity: Proceedings of the 5th North American Rock Mechanics Symposium and the 17th Tunnelling Association of Canada Conference, NARMS–TAC 2002, Toronto, Ont., 7–10 July 2002. University of Toronto Press, Toronto, Ont., Vol. 1, pp. 267–273.

Holtz, R.D., and Kovacs, W.D. 1981. An introduction to geotechnical engineering. Prentice Hall Inc., Englewood Cliffs, N.J.

Höskuldsson, A., and Sparks, R.S.J. 1997. Thermodynamics and fluid dynamics of effusive subglacial eruptions. Bulletin of Volcanology, **59**: 219–231.

International Society for Rock Mechanics Commission on Standardization of Laboratory and Field Tests. 1978. Suggested methods for the quantitative description of discontinuities in rock masses. International Journal of Rock Mechanics and Mining Sciences and Geomechanics Abstracts, **15**: 319–368.

Ishijima, Y., and Fujii, Y. 1997. A study of the mechanism of slope failure at Toyohama Tunnel, 10 February 1996. International Journal of Rock Mechanics and Mining Sciences, **34**: 519.

Jones, J.G. 1969. Intraglacial volcanoes of the Laugarvatn region, south-west Iceland — I. Quarterly Journal of the Geological Society (of London), **124**: 197–211.

Jones, J.G. 1970. Intraglacial volcanoes of the Laugarvatn region, southwest Iceland, II. Journal of Geology, **78**: 127–140.

Komatsu, G., Ori, G.G., Ciarcelluti, P., and Litasov, Y.D. 2004. Interior layered deposits of Valles Marineris, Mars: analogous subice volcanism related to Baikal Rifting, southern Siberia. Planetary and Space Science, **52**: 167–187.

Le Masurier, W.E. 2002. Architecture and evolution of hydrovolcanic deltas in Marie Byrd Land, Antarctica. *In* Volcano–ice interactions on Earth and Mars. *Edited by* J.L. Smellie and M.G. Chapman. Geological Society (of London) Special Publication 202, pp. 115–148.

Lockner, D.A. 1995. Rock failure. *In* Rock physics and phase relations: a handbook of physical constants. *Edited by* T.J. Ahrens. American Geophysical Union, Reference Shelf 3, pp. 127–147.

Mathews, W.H. 1947. "Tuyas," flat-topped volcanoes in northern British Columbia. American Journal of Science, **245**: 560–570.

Rahn, P.H. 1996. Engineering geology: an environmental approach. Prentice Hall Inc., Englewood Cliffs, N.J.

Ritter, D.F., Kochel, R.C., and Miller, J.R. 1995. Process geomorphology. Wm.C. Brown, Dubuque, Iowa.

Skilling, I.P. 1994. Evolution of an englacial volcano: Brown Bluff, Antarctica. Bulletin of Volcanology, **56**: 573–591.

Smellie, J.L. 2000. Subglacial eruptions. *In* Encyclopedia of volcanoes. *Edited by* H. Sigurdsson. Academic Press, New York, N.Y., pp. 403–418.

Smellie, J.L. 2002. The 1969 subglacial eruption on Deception Island (Antarctica): events and processes during an eruption beneath a thin glacier and implications for volcanic hazards. *In* Volcano–ice interactions on Earth and Mars. *Edited by* J.L. Smellie and M.G. Chapman. Geological Society (London), Special Publication 202, pp. 59–79.

Smellie, J.L., and Hole, M.J. 1997. Products and processes in Pliocene–Recent, subaqueous to emergent volcanism in the Antarctic Peninsula: examples of englacial Surtseyan volcano construction. Bulletin of Volcanology, **58**: 628–646.

Smellie, J.L., and Skilling, I.P. 1994. Products of subglacial volcanic eruptions under different ice thicknesses: two examples from Antarctica. Sedimentary Geology, **91**: 115–129.

Smellie, J.L., Hole, M.J., and Nell, P.A.R. 1993. Late Miocene valley-confined subglacial volcanism in northern Alexander Island, Antarctic Peninsula. Bulletin of Volcanology, **55**: 273–288.

Sonmez, H., and Ulusay, R. 1999. Modifications to the geological strength index (GSI) and their applicability to stability of slopes. International Journal of Rock Mechanics and Mining Sciences, **36**: 743–760.

Van Bemmelen, R.W., and Rutten, M.G. 1955. Table mountains of Northern Iceland. E.J. Brill, Leiden, The Netherlands.

Walker, S.R., and Santi, P.M. 2004. Influence of the Blue Mesa Reservoir on the Red Creek Landslide, Colorado. Environmental and Engineering Geoscience, **10**: 13–26.

Werner, R., and Schmincke, H.-U. 1999. Englacial vs. lacustrine origin of volcanic table mountains: evidence from Iceland. Bulletin of Volcanology, **60**: 335–354.